SAGA-HE-79-95
February 1995

Effective nucleon mass, incompressibility and third-order derivative of nuclear saturation curve in the relativistic mean field theory with vector meson self-interaction

H. Kouno, K. Koide, T. Mitsumori, N. Noda, A. Hasegawa
and
M. Nakano*

Department of Physics, Saga University, Saga 840, Japan

**University of Occupational and Environmental Health, Kitakyushu 807, Japan*

ABSTRACT

The relations among the effective nucleon mass M_0^*, incompressibility K and the third-order derivative K' of saturation curve are studied using the relativistic mean field model which has both the scalar and the vector self-coupling interactions. The vector self-coupling makes the EOS softer at higher densities when $K \gtrsim 200$MeV. The Coulomb coefficient K_c of nucleus incompressibility is also calculated. The parameters sets of the model are determined so as to realize both the empirical K-K_c relation and $M_0^* = 0.6M$ which is consistent with the empirical spin-orbit potential. The obtained EOS with $K = 300$MeV is successful to account for the symmetry properties and very close to the results of the Dirac-Brueckner-Hartree-Fock calculation.

I. INTRODUCTION

One way to determine the incompressibility K of nuclear matter from the giant monopole resonance (GMR) data is using the leptodermous expansion[1] of nucleus incompressibility $K(A,Z)$ as follows.

$$K(A,Z) = K + K_{sf}A^{-1/3} + K_{vs}I^2 + K_c Z^2 A^{-4/3} + \cdots \quad ; \quad I = 1 - 2Z/A, \qquad (1)$$

where the coefficients K_{sf}, K_{vs} and K_c are surface term coefficient, volume-symmetry coefficient and Coulomb coefficient respectively. We have omitted higher terms in eq. (1). Though there is uncertainty in the determination of these coefficients by using the present data, Pearson [2] pointed out that there is a strong correlation among K, K_c and the skewness coefficient, i.e., the third-order derivative of nuclear saturation curve. Similar observations are done by Shlomo and Youngblood [3].

According to this context, Rudaz et al. [4] studied the relation between K and the skewness coefficient using the generalized version of the relativistic Hartree approximation [5]. Recently, both of compressional and surface properties are studied by Von-Eiff et al. [6][7][8] in the framework of the mean field approximation of the σ-ω-ρ model with the nonlinear σ terms. They found that low incompressibility ($K \approx 200$MeV) and a large effective nucleon mass M_0^* at the normal density ($0.70 \leq M_0^*/M \leq 0.75$) are favorable for the nuclear surface properties [8]. On the other hand, using the same model, Bodmer and Price [9] found that the experimental spin-orbit splitting in light nuclei supported $M_0^* \approx 0.60M$. The result of the generator coordinate calculations for breathing-mode GMR by Stoitsov, Ring and Sharma [10] suggests that $K \approx 300$MeV.

In previous paper[11], we have studied the relation between K and the third-order derivative K' of nuclear saturation curve in detail, using the mean field theory with the nonlinear σ terms [12]. We found that $K = 300$MeV is favorable to account for K, K_c, a_4 and K_{vs}, simultaneously. However, the effective nucleon mass M_0^* of the equations of state (EOS) which we found is $0.83M$. That is larger than the value of the analysis by Bodmer and Price [9], which is referred above.

In this paper, we study the effective nucleon mass, incompressibility K and K', using the mean field theory which has the vector self-interaction as well as the scalar self-interactions [13], and compare the results with the GMR data empirically, under the assumption of scaling model[1]. It is known that the EOS of the relativistic mean field theory with vector self-coupling is very close to the result of the Dirac-Bruecner-Hartree-Fock (DBHF) calculations [14] [15] even at the higher densities [16][17]. This

paper is organized as follows. In section 2, we review the general formalism of the vector self-coupling model, briefly. In section 3, the saturation condition is investigated, and the expressions for K and K' are shown. In section 4, the relation among M_0^*, K and K' is studied. In sect. 5, the parameters of the model are determined so as to account for both the empirical K-K_c relation and the empirical spin-orbit potential [13]. Section 6 is devoted to the summary of this paper.

II. FORMALISM

We use the nonlinear relativistic mean field theory based on the σ-ω model with nonlinear σ and ω terms [13]. (For a while, we restrict our discussions to the symmetric nuclear matter and do not consider the ρ meson effects.) The lagrangian density consists of three fields, the nucleon ψ, the scalar σ-meson ϕ and the vector ω-meson V_μ, i.e.,

$$L = \bar{\psi}(i\gamma_\mu\partial^\mu - M)\psi + \frac{1}{2}\partial_\mu\phi\partial^\mu\phi - \frac{1}{4}F_{\mu\nu}F^{\mu\nu} + \frac{1}{2}m_v^2 V_\mu V^\mu(1 + \frac{g_v^2}{2}Y^2 V_\mu V^\mu)$$

$$+ g_s\bar{\psi}\psi\phi - g_v\bar{\psi}\gamma_\mu\psi V^\mu - U(\phi) \quad ; \qquad F_{\mu\nu} = \partial_\mu V_\nu - \partial_\nu V_\mu, \qquad (2)$$

where m_v, g_s and g_v are ω-meson mass, σ-nucleon coupling and ω-nucleon coupling respectively. The potential $U(\phi)$ includes a nonlinear cubic-quartic terms of the scalar field ϕ; i.e.,

$$U(\phi) = \frac{1}{2}m_s^2\phi^2 + \frac{1}{3}b\phi^3 + \frac{1}{4}c\phi^4, \qquad (3)$$

where m_s is σ-meson mass, and b and c are the constant parameters which are determined phenomenologically. The constant parameter Y represents the strength of the vector self-interaction. In the mean field approximation, the effective nucleon mass M^* is given by

$$M^* = M - \Phi \quad : \qquad \Phi = g_s < \phi >, \qquad (4)$$

where $< \phi >$ is the ground-state expectation value of the field ϕ. The baryon density ρ and scalar density ρ_s are given by

$$\rho = \frac{\lambda}{3\pi^2}k_F^3, \qquad (5)$$

and

$$\rho_s = \frac{\lambda}{2\pi^2}M^*[k_F\sqrt{k_F^2 + M^{*2}} - M^{*2}\ln(\frac{k_F + \sqrt{k_F^2 + M^{*2}}}{M^*})], \qquad (6)$$

where k_F is the Fermi momentum and $\lambda = 2$ in nuclear matter. The total energy of the system is also given by

$$\epsilon = \epsilon_N + \epsilon_v + U(\Phi). \tag{7}$$

The nucleon energy term ϵ_N in eq. (7) is given by

$$\epsilon_N(k_F, M^*) = \frac{\lambda}{12\pi^2}[3k_F^3 E_F^* + \frac{3}{2}M^{*2}k_F E_F^*$$

$$-\frac{3}{2}M^{*4}\ln(\frac{k_F + E_F^*}{M^*})], \tag{8}$$

where $E_F^* = \sqrt{k_F^2 + M^{*2}}$. The vector meson part ϵ_v is given by

$$\epsilon_v = W\rho - \frac{1}{2}\frac{M^2W^2}{C_v^2}(1 + \frac{Y^2W^2}{2}); \qquad W = g_v < V^0 >, \tag{9}$$

where $< V^0 >$ is the ground-state expectation value of V^0 and $C_v = g_v M/m_v$. In the latter part of this paper, we write $U(\Phi)$ as

$$U(\Phi) = \frac{1}{2C_s^2}M^2\Phi^2 + \frac{1}{3}BM\Phi^3 + \frac{1}{4}C\Phi^4, \tag{10}$$

where $C_s = g_s M/m_s$, $B = b/(g_s^3 M)$ and $C = c/g_s^4$.

The equation for the scalar field is expressed as

$$U'(\Phi) = \frac{dU(\Phi)}{d\Phi} = \frac{1}{C_s^2}M^2\Phi + BM\Phi^2 + C\Phi^3 = \rho_s. \tag{11}$$

Using eqs. (4), (6) and (11), we can determined M^* and Φ in a self-consistent way.

The W can be determined by the equation of motion for the vector field,

$$\frac{\partial \epsilon_v}{\partial W} = 0. \tag{12}$$

The equation (12) gives [13]

$$w(1 + w^2) - y' = 0, \tag{13}$$

where $w = WY$ and $y' = C_v^2\rho Y/M^2$ are dimensionless quantities. When $y'(\geq 0)$ is

given, the equation (13) has a non-negative real solution as

$$w = \sqrt[3]{\frac{\sqrt{D} + y'}{2}} - \sqrt[3]{\frac{\sqrt{D} - y'}{2}}, \tag{14}$$

where $D = y'^2 + 4/27$. Because $d(w(1 + w^2) - y')/dw = 1 + 3w^2 > 0$, eq. (14) is the unique real solution of eq. (13). In the case of $y'^2 >> 4/27$, $w \approx y'^{1/3}$. When M^*, Φ and W are determined, we can calculate energy density of the system given by eq. (7).

III. SATURATION CONDITION, INCOMPRESSIBILITY AND THIRD-ORDER DERIVATIVE OF NUCLEAR SATURATION CURVE

At the saturation density ρ_0, the pressure P of the system vanishes, i.e.,

$$P = \rho^2\frac{de}{d\rho} = \rho(W + E_F^* - e) = 0 \quad ; \qquad e = \frac{\epsilon}{\rho}. \tag{15}$$

The saturation condition (15) gives the following relation [13]

$$W_0 = W(\rho = \rho_0) = \frac{w_0}{Y} = \frac{C_v^2\rho_0 w_0}{M^2 y} = e_0 - E_F^* = -a_1 + M - \sqrt{k_{F0}^2 + M_0^{*2}}, \tag{16}$$

where $y = C_v^2\rho_0 Y/M^2$ and the values with the subscript "0" are the ones at the normal density ρ_0. We remark $y = y'(\rho = \rho_0)$. The equation (16) is written as

$$M_0^* = \sqrt{(-a_1 + M - \frac{C_v^2\rho_0 w_0}{M^2 y})^2 - k_{F0}^2}, \tag{17}$$

or [13]

$$C_v^2 = (-a_1 + M - \sqrt{k_{F0}^2 + M^{*2}})yM^2/(w_0\rho_0). \tag{18}$$

Putting $C_v = 0$ and $\rho_0 = 0.15\text{fm}^{-3}$ in eq. (17), we get $M^* \approx 0.94M$ which is the upper bound for M_0^* in this model. Using eq. (18), in fig. 1, we show the relation between y and C_v^2 with several values of M_0^*. When y becomes larger, C_v becomes larger when M_0^* is fixed. From the discussion in the end of the previous section, $w_0 \approx y^{1/3}$ for the large $y(y^2 >> 4/27)$. Then, C_v^2 is proportional to $y^{2/3}$ in the large y limit.

Fig. 1

The incompressibility K at the normal density is defined as

$$K = 9\rho_0^2 \frac{\partial^2 e}{\partial \rho^2}|_{\rho=\rho_0} = 9\frac{\partial P}{\partial \rho}|_{\rho=\rho_0} = 9\rho_0 \frac{\partial \mu}{\partial \rho}|_{\rho=\rho_0}, \tag{19}$$

where the baryonic chemical potential μ is given by

$$\mu = E_F^* + W. \tag{20}$$

In this model, K is written as [13]

$$K = 9\rho_0 \Big(\frac{C_v^2}{M^2(1+3w^2)} + \frac{k_F^2}{3\rho E_F^*} + \frac{M^*}{E_F^*} M^{*\prime} \Big)_{\rho=\rho_0}, \tag{21}$$

where

$$M^{*\prime} = \frac{dM^*}{d\rho} = -\frac{M^*}{E_F^*} \frac{1}{U''(\Phi) + \partial\rho_s/\partial M^*}, \tag{22}$$

with

$$U''(\Phi) = \frac{d^2 U(\Phi)}{d\Phi^2}. \tag{23}$$

From eq. (6), $\partial\rho_s/\partial M^*$ is given by

$$\frac{\partial \rho_s}{\partial M^*} = \frac{\lambda}{2\pi^2}[k_F E_F^* - 3M^{*2} \ln\big(\frac{k_F + E_F^*}{M^*}\big) + 2\frac{k_F M^{*2}}{E_F^*}]. \tag{24}$$

We also defined the third-order derivative K' of nuclear binding energy $E_b(= e - M)$ as

$$K' = 3\rho_0^3 \frac{d^3 E_b}{d\rho^3}|_{\rho=\rho_0} = 3\rho_0 \frac{d^2 P}{d\rho^2}|_{\rho=\rho_0} - \frac{4}{3}K = 3\rho_0^2 \frac{d^2 \mu}{d\rho^2}|_{\rho=\rho_0} - K. \tag{25}$$

In this model, K' is written as

$$K' = 3\rho_0^2 \Big(-\frac{6wy}{\rho_0 M^2} \frac{C_v^2}{(1+3w^2)^3} + \frac{d^2 E_F^*}{d\rho^2} \Big)_{\rho=\rho_0} - K, \tag{26}$$

where

$$\frac{d^2 E_F^*}{d\rho^2} = \frac{1}{E_F^*}[(\frac{k_F M^*}{3\rho E_F^*})^2 + (\frac{k_F}{E_F^*} M^{*\prime})^2 - 2\frac{k_F^2 M^*}{3\rho E_F^{*2}} M^{*\prime} - \frac{2k_F^2}{9\rho^2} + M^* M^{*\prime\prime}]. \tag{27}$$

The $M^{*\prime\prime} = \frac{d^2 M^*}{d\rho^2}$ is given by

$$(U''(\Phi) + \frac{\partial \rho_s}{\partial M^*}) M^{*\prime\prime} = -\frac{1}{E_F^*} M^{*\prime} + \frac{k_F^2 M^*}{3\rho E_F^{*3}} + \frac{M^{*2}}{E_F^{*3}} M^{*\prime} + (M^{*\prime})^2 U^{(3)}(\Phi) - \frac{d}{d\rho}(\frac{\partial \rho_s}{\partial M^*}) M^{*\prime}, \tag{28}$$

where

$$\frac{d}{d\rho}(\frac{\partial \rho_s}{\partial M^*}) = \frac{\lambda}{2\pi^2}[(3k_F - 2E_F^* + 2\frac{M^{*2}}{E_F^*})\frac{k_F}{3\rho} + (4k_F - 3E_F^* - 2\frac{k_F M^{*2}}{E_F^{*2}})(\frac{k_F^2}{3E_F^* \rho} + \frac{M^*}{E_F^*} M^{*\prime})$$

$$+ (3M^* + 4\frac{k_F M^*}{E_F^*} - 6M^* \ln[\frac{k_F + E_F}{M^*}]) M^{*\prime}], \tag{29}$$

and

$$U^{(3)} = \frac{d^3 U(\Phi)}{d\Phi^3}. \tag{30}$$

IV. THE RELATION AMONG THE EFFECTIVE NUCLEON MASS, INCOMPRESSIBILITY AND THE THIRD-ORDER DERIVATIVE OF NUCLEAR SATURATION CURVE

In our calculations, we put M = 939MeV, $\rho_0 = 0.15\mathrm{fm}^{-3}$ and a_1 = 15.75MeV. The other independent parameters y, C_s, C_v, B and C are determined phenomenologically. Besides the two conditions for saturation, i.e., $e_0 = M - a_1$ and $P = 0$, when M_0^*, K and K' are given, we can determine the five parameters of the model. The M_0^* depends on only y and C_v as is seen in eq. (17). Therefore, we give one (two) quantity (quantities) among y, C_v and M_0^* and give two (one) quantities (quantity) among C_s, B, C, K and K'. The other quantities are automatically determined.

First, we check the sign of the quartic coefficient C of the scalar potential $U(\Phi)$, because the negative value of C may cause undesirable behaviors such as bifurcation of the solution [13]. As is pointed out in ref. [13], the vector self-coupling makes C less negative. In fig. 2. we show the regions for $C > 0$ in the K-M_0^* plane with several values of y. The region is widened as y becomes larger. The C becomes larger (more repulsive) to cancel the attractive effect of vector self-coupling in ϵ_v (See eq. (9)). In the case of $y \geq 2$, C is positive for $M_0^* \geq 0.5M$ and $K = 150 \sim 400$MeV.

Fig. 2

Fig. 3(a),(b)

Fig. 4(a),(b)

In fig. 3, we show the $M_0^* - K'$ relations with fixed values of K both in the cases of $y = 0$ and $y = 1.0$. When $y = 1.0$, K' monotonically decreases as M_0^* increases. The cross points of curves at $M_0^* \sim 0.8M$, which appear in the case of no vector self-coupling, disappear when $y = 1.0$. In the cases with $y = 1.0$ and $M_0^* \gtrsim 0.6M$, K' is negative. When $K \geq 200$MeV, K' with $y = 1.0$ is smaller than that with $y = 0$. It seems that the vector self-coupling makes EOS of nuclear matter softer at higher densities. To confirm this observations, in fig. 4, we show the y-dependence of $K - K'$ relation when $M_0^* = 0.6M$ or $0.8M$. When $K \gtrsim 200$MeV and $M_0^* = 0.6M$, the vector self-coupling makes K' smaller. In the case of $M_0^* = 0.8M$, K' decreases as y increases for any K. The vector self-coupling makes equations of state of nuclear matter softer at higher densities. However, the $K - K'$ relations hardly change in the larger y limit ($y > 2$).

To compare these results with experiments of GMR, we calculate the Coulomb coefficient K_c of the leptodermous expansion (1), using the scaling model, i.e., using the following equation [1],

$$K_c = -\frac{3q_{el}^2}{5r_0}\left(\frac{9K'}{K} + 8\right), \tag{31}$$

where q_{el} is the electric charge of proton and $r_0 = (3/(4\pi\rho_0))^{1/3}$. In fig. 5, we show the $K - K_c$ relations with several values of M_0^* in the cases of $y = 0$ and $y = 1.0$. When $K \gtrsim 200$M, the vector self-coupling makes K_c less negative because of the decrease of the ratio K'/K. In these cases, we can account for the empirical values using the vector coupling and the smaller M_0^*. On the contrary, when $K \lesssim 200$MeV, the vector self-coupling does not make K'/K much smaller or makes K'/K larger. Therefore, it does

not make K_c much larger or makes K_c smaller. So we can not account for the empirical values for $K < 200$MeV even we make y larger.

Fig. 5(a),(b)

V. Determinations of parameters and symmetry properties

In this section, we determined the parameters of our model, using the empirical data by Pearson [2]. In table I, we show the set of the empirical values of K and K_c in table 3 of ref. [2]. According to the conclusion of ref. [2], i.e., $K = 120 \sim 351$MeV, we only show the sets with $K = 150 \sim 350$MeV. In fig. 6, we show the $y - M_0^*$ relations which account for the sets. We could not find the parameters for sets with $K = 150$MeV and for the set with $K = 200$MeV and $K_c = 2.577, 2.577 + 2.06$MeV as in the cases of $y = 0$ [11], because of the reason which is mentioned in the end of the previous section. The M_0^* decreases as y increases in any case of K.

Table I

Fig. 6

The smaller M_0^* and the larger y has the opposite effects to the larger y in the EOS. The smaller M_0^* makes the EOS stiffer, while the smaller y makes the EOS softer. In fig. 7, we show the EOS with several y, which account for the set of $K = 250$MeV and $K_c = -0.7065$MeV. The EOS becomes softer when $y = 0.5$, because the effect of larger y is larger than the effect of smaller M_0^*. The EOS becomes stiffer again when $y = 1.0$, because, as is shown in fig. 6, the M_0^* decreases rapidly enough to overcome the larger y effect. Though we do not show a figure, two effects almost cancel each other in the case of $K = 300$MeV and $K_c = -3.990$MeV, when y is not so large ($y \lesssim 5$).

Fig. 7

Table II

In this vector self-coupling theory, there is one more input to fix the EOS. According to ref. [13], $M_0^* \approx 0.6M$ is favorable to account for the spin-orbit potential and the optical potential. We search for the parameters sets which account for the data sets in table I and $M_0^* = 0.6M$. The results are summarized in table II. It is impossible to find the parameters for the sets of $(K, K_c) = (350, -7.274)$MeV,$(350, -7.274 - 2.06)$MeV, because, as shown in fig. 6, in these cases M_0^* is always smaller than $0.6M$ at any y. (For comparison, in table II we also show the EOS with the parameters set which satisfies $K = 350$MeV, $K = -7.274$MeV and $y = 0$, whose $M_0^*(= 0.597M)$ is very close to $0.6M$. We call this parameters set EOS 6.) Also we could not find the parameter sets for $K \geq 250$MeV, except EOS 1, in the region $y < 10$. It seem to be difficult to find these parameters even if we make y larger. It is probably because, as is seen in fig. 6, M_0^* hardly decreases in the larger y region. We remark that $C > 0$ except for the cases of the EOS 4 and 6.

If we fix M_0^*, there is still uncertainty of K. To determine K, we calculate the volume-symmetry coefficient K_{vs} in the expansion (1). Because the ρ-meson effects is important in the symmetry properties [18][19], we add the following standard ρ-meson-term to the lagrangian (2)[18][19][17].

$$L_\rho = -\frac{1}{4}\mathbf{B}_{\mu\nu}\cdot\mathbf{B}^{\mu\nu} + \frac{1}{2}m_\rho^2\mathbf{b}_\mu\cdot\mathbf{b}^\mu - g_\rho\bar{\psi}\gamma_\mu\frac{\tau}{2}\cdot\mathbf{b}^\mu\psi; \quad \mathbf{B}_{\mu\nu} = \partial_\mu\mathbf{b}_\nu - \partial_\nu\mathbf{b}_\mu - g_\rho\mathbf{b}_\mu\times\mathbf{b}_\nu, \quad (32)$$

where $\mathbf{b}$ is the ρ meson field. Using the new lagrangian and the mean field approximation, we can calculate K_{vs} with aid of the scaling model [1]

$$K_{vs} = K_{sym} - L\left(9\frac{K'}{K} + 6\right), \quad (33)$$

where

$$L = 3\rho_0\frac{da_4}{d\rho}|_{\rho=\rho_0}; \qquad a_4 = \frac{1}{2}\rho\frac{\partial^2\epsilon}{\partial\rho_3^2}|_{\rho_3=0}; \qquad \rho_3 = \rho_p - \rho_n \quad (34)$$

and

$$K_{sym} = 9\rho_0^2\frac{d^2a_4}{d\rho^2}|_{\rho=\rho_0}. \quad (35)$$

The results are also summarized in table II. In these calculations, we determine the ρ meson coupling g_ρ so as to realize $a_4 = 30.0$MeV at $\rho = \rho_0$. However, the results do not depend much on the choise of g_ρ, because K_{vs} is more sensitive to the ratio K'/K

than to g_ρ. In fact, if we put $C_\rho^2 = (g_\rho M/m_\rho)^2 = 50 \sim 100$ in the EOS 3, we get $K_{vs} \approx -258 \sim -340$MeV. The difference is not larger than the length of empirical error bar (202MeV) in ref. [2]. In fig. 8, we compare these results with the empirical data in refs. [2] and [3]. From the figure, it is seen that EOS 1 and 3 are favorable to account for the empirical values of K_{vs}, though the EOS 5 could not be excluded. The EOS 3($K = 300$MeV) is most favorable as in the case of $y = 0$ [11], because it corresponds to the mean value of the empirical K_c.

In fig. 9, we show the k_F-dependence of nuclear binding energy using the EOS 1,3 and 5. The result of the EOS 3 is much closer to the EOS of the DBHF calculations [14] than the EOS of the mean field theories with the NL1 parameters [20] and with the NL-SH parameters [21], which do not have the vector self-coupling. This is consistent with the observations by Gmuca [16] and by Sugahara and Toki[17].

Fig. 8

Fig. 9

VI. SUMMARY

We studied the relations among the effective nucleon mass M_0^*, incompressibility K, the third-order derivative K' of nuclear saturation curve, using the mean field theory with the vector self-coupling. The results are summarized as follows.

(1) When we fix M_0^* and $K(\gtrsim 200$MeV), the vector self-coupling makes K' smaller, i.e., makes the EOS softer at higher densities.

(2) Using the vector self-coupling, we can account for the empirical relation between $K(\gtrsim 250$MeV) and K_c with the smaller M_0^*.

(3) We could not find the parameters for the empirical sets $(K, K_c) = (150, 5.861 \pm 2.06)$MeV, $(200, 2.577)$MeV and $(200, 2.577 + 2.06)$MeV, when $y < 10$. It is due to the fact that the vector self-coupling does not make K' much smaller when $K \lesssim 200$MeV.

(4) It seems that $(K, K_c) = (300, -3.990)$MeV is favorable to account for the symmetry properties besides the empirical K-K_c relations.

(5) The EOS which is given by parameter set in (4) has very close to the RBHF's EOS at the higher densities.

In this paper, we restrict our discussions to the M_0^*, K, K', K_c and K_{vs}, because they can be calculated in the framework of the nuclear matter and do not depend parameter m_σ. Von-Eiff et al. studied the surface properties [6][7][8] in the framework of the mean field approximation of the nonlinear σ-ω-ρ model with no vector self-coupling (i.e, in the case of $y = 0$). They found that low incompressibility ($K_{nm} \approx 200$MeV) and a large effective nucleon mass ($0.70 \leq M^*/M \leq 0.75$) are favorable for the nuclear surface properties [8]. It is interesting to study these problem using the vector self-coupling model.

Acknowledgment: Authors are grateful to Prof. Kohmura, Prof. Sakaguchi, Prof. Kumano, N. Fukunishi and N. Kakuta for useful discussions, and to the members of nuclear theorist group in Kyushyu district in Japan for their continuous encouragement. The authors also gratefully acknowledge the computing time granted by the Research Center for Nuclear Physics (RCNP).

References

[1] J.P. Blaizot, Phys. Rep. **64** ,171(1980).

[2] J.M. Pearson, Phys. Lett. B**271** ,12(1991).

[3] S. Shlomo and D.H. Youngblood, Phys. Rev.C**47** ,529(1993).

[4] S. Rudaz, P.J. Ellis, E.K. Heide and M. Prakash, Phys. Lett. **B285**, 183(1992).

[5] E.K. Heide and S. Rudaz, Phys. Lett. **B262**, 375(1991).

[6] D. Von-Eiff, J.M. Pearson, W. Stocker and M.K. Weigel, Phys Lett. **B324**, 279(1994).

[7] D. Von-Eiff, J.M. Pearson, W. Stocker and M.K. Weigel, Phys. Rev. **C50**, 831(1994).

[8] D. Von-Eiff, W. Stocker and M.K. Weigel, Phys. Rev. **C50**, 1436(1994).

[9] A.R. Bodmer and C.E. Price, Nucl. Phys. **A505**, 123(1989).

[10] M.V. Stoitsov, P. Ring and M.M. Sharma, Phys. Rev. **C50**, 1445(1994).

[11] H. Kouno et al., to be published in Phys. Rev. C.

[12] J. Boguta and A.R. Bodmer, Nucl. Phys. **A292**, 413(1977)

[13] A.R. Bodmer, Nucl. Phys. **A526**, 703(1991).

[14] R. Brockmann and R. Machleidt, Phys. Rev. **C42**, 1965(1990).

[15] F. de Jong and R. Malfliet, Phys. Rev. **C44**, 998(1991).

[16] S. Gmuca, Nucl. Phys. **A547**, 447(1992).

[17] Y. Sugahara and H. Toki, Nucl. Phys. **A579**, 557(1994).

[18] B.D. Serot, Phys. Lett. B**86**, 146(1979)

[19] B.D. Serot and J.D. Walecka, *The Relativistic Nuclear Many-Body Problem* in: Advances in nuclear physics, vol. 16 (Plenum Press, New York, 1986).

[20] P.-G. Reinhard, Rep. Prog. Phys. **52**, 439(1989)

[21] M.M. Sharma, M.A. Nagarajan and P. Ring, Phys. Lett. B**312**, 377(1993)

	Set 1	Set 2	Set 3	Set 4	Set 5
K	150	200	250	300	350
K_c	5.861 ± 2.06	2.577 ± 2.06	-0.7065 ± 2.06	-3.990 ± 2.06	-7.274 ± 2.06

Table I

EOS	1	2	3	4	5	6
K	250	300	300	300	350	350
K_c	-0.7065-2.06	-3.990+2.06	-3.990	-3.990-2.06	-7.274+2.06	-7.274
K'	-118.2	-179.6	-86.68	6.237	-36.72	71.69
M_0^*/M	0.600	0.600	0.600	0.600	0.600	0.597
K_{vs}	-165.2	-75.23	-299.7	-524.0	-437.5	-667.0
L	82.96	81.82	87.29	93.03	90.48	95.42
K_{sym}	-20.51	-25.18	-2.977	51.61	19.94	81.40
y	1.974	2.459	0.7096	0.2493	0.3849	0.000
C_s^2	516.45	477.19	387.91	352.63	350.30	338.39
C_v^2	464.44	519.65	303.52	246.76	261.41	235.83
B	-1.378×10^{-3}	-3.697×10^{-3}	-5.820×10^{-4}	1.207×10^{-3}	-5.019×10^{-5}	1.260×10^{-3}
C	1.177×10^{-2}	1.657×10^{-2}	5.767×10^{-3}	-3.167×10^{-4}	2.708×10^{-3}	-1.372×10^{-3}

Table II

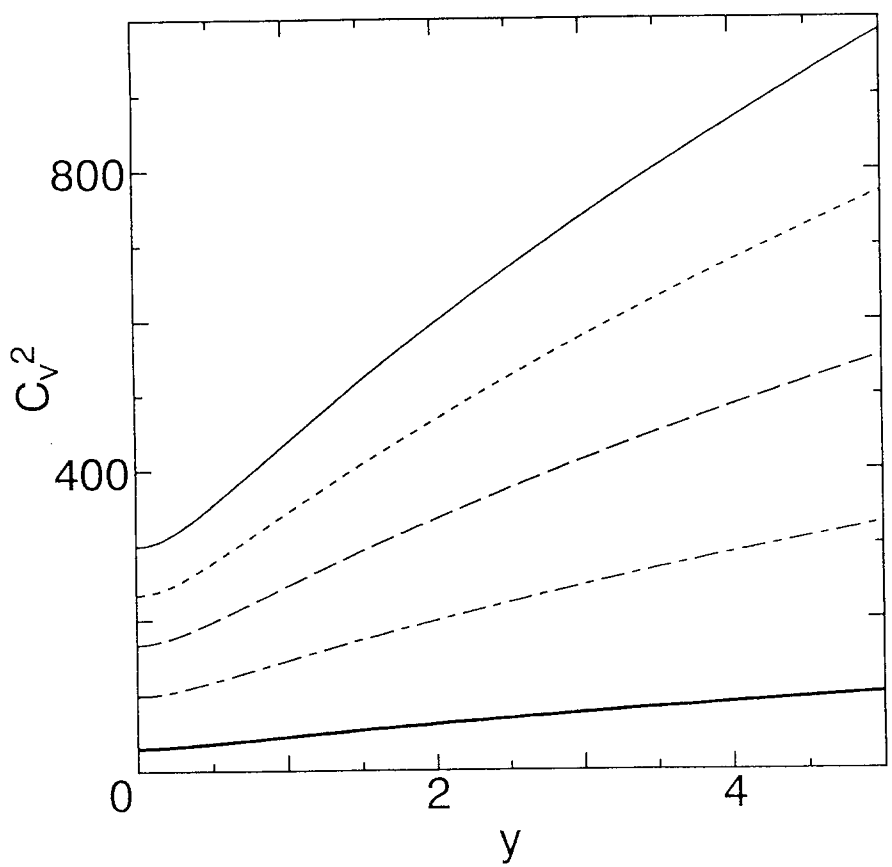

fig.1

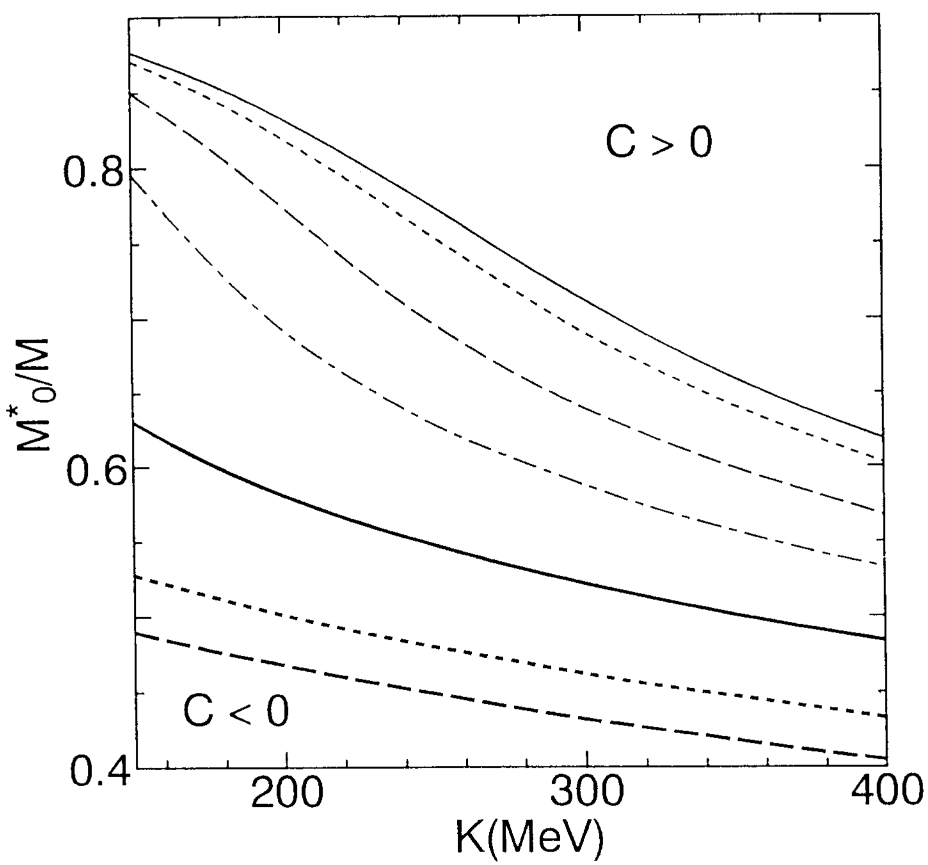

fig.2

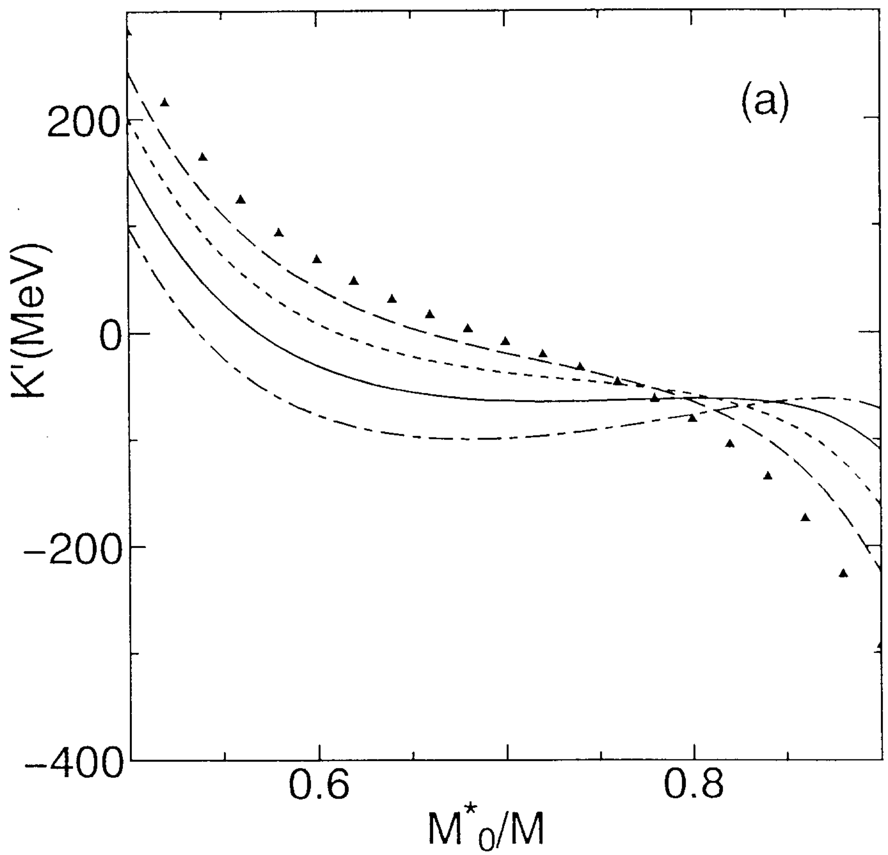

fig.3(a)

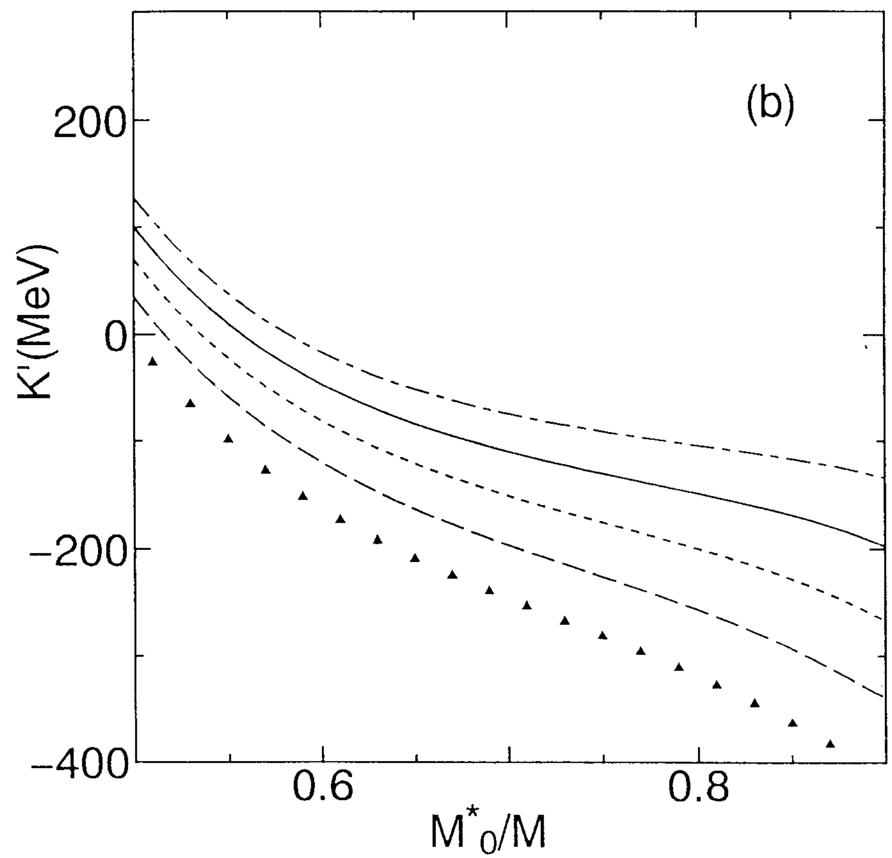

fig.3(b)

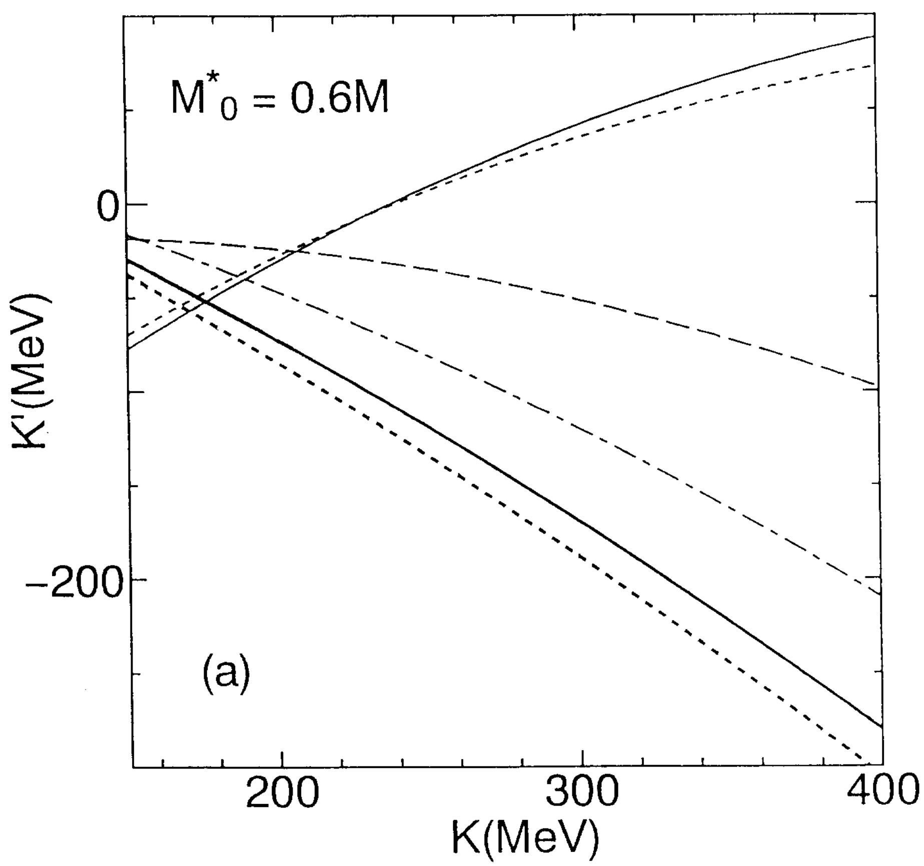

M*0 = 0.6M
0
−200
(a)
200
300
400
K(MeV)
K'(MeV)

fig.4(a)

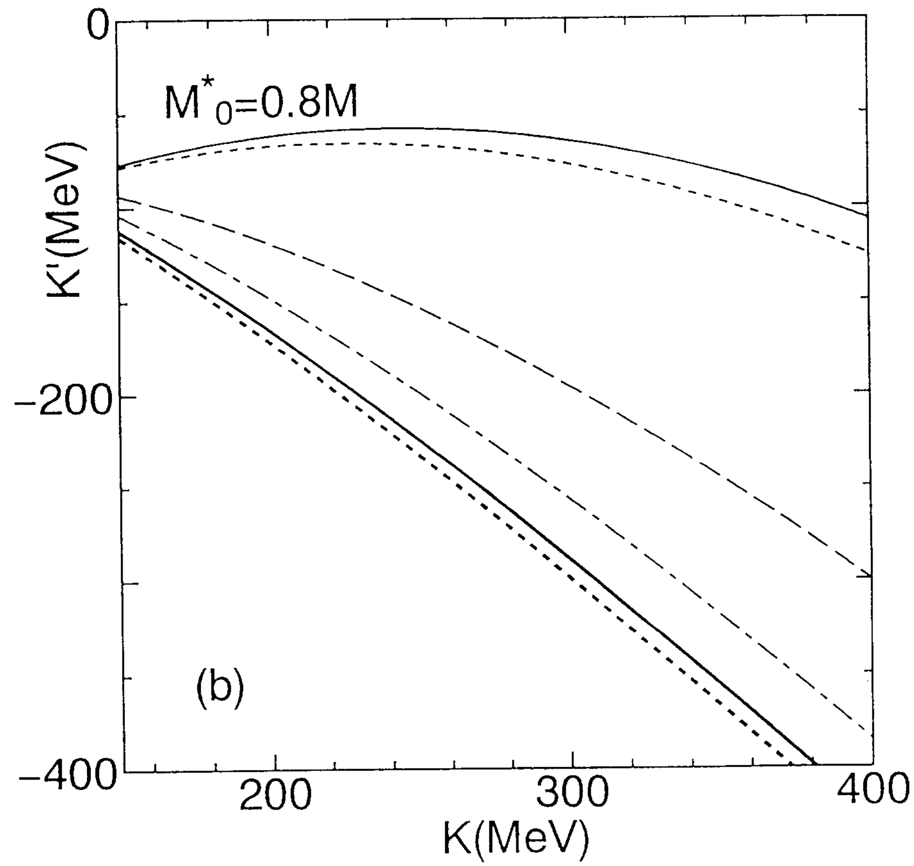

0
M*0=0.8M
−200
−400
(b)
200
300
400
K(MeV)
K'(MeV)

fig.4(b)

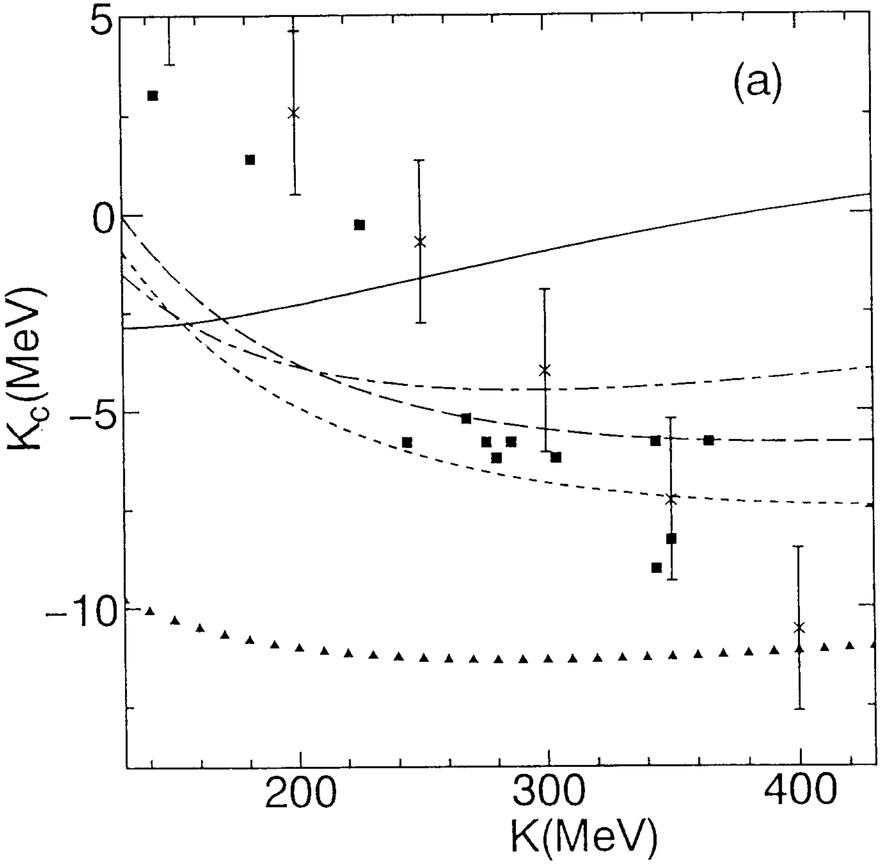

fig.5(a)

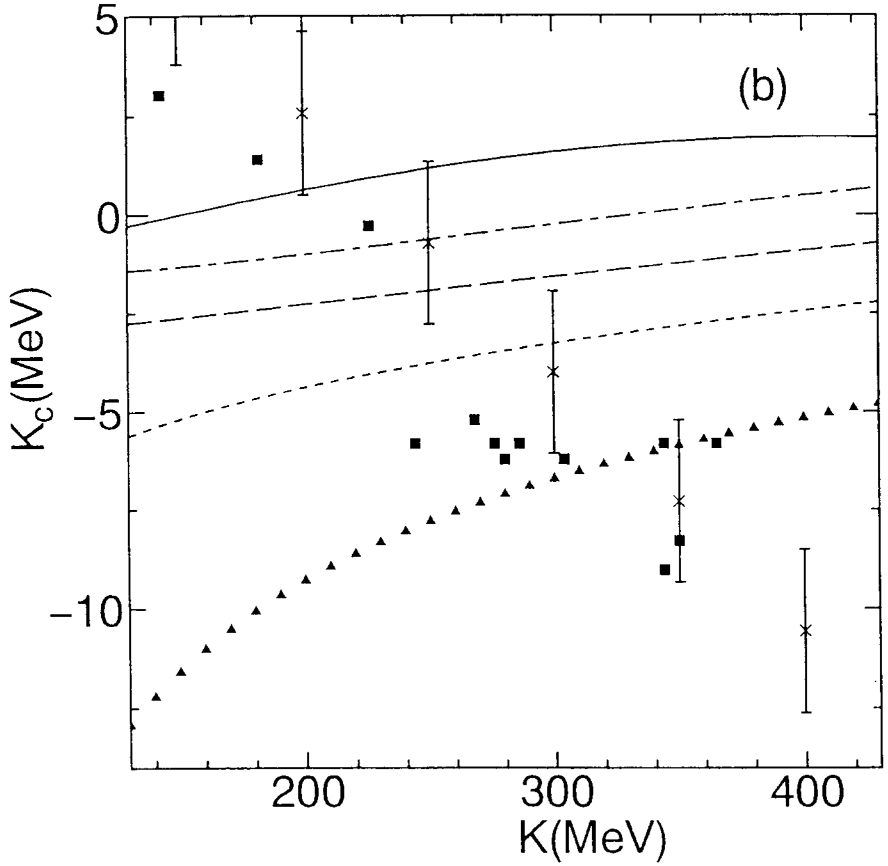

fig.5(b)

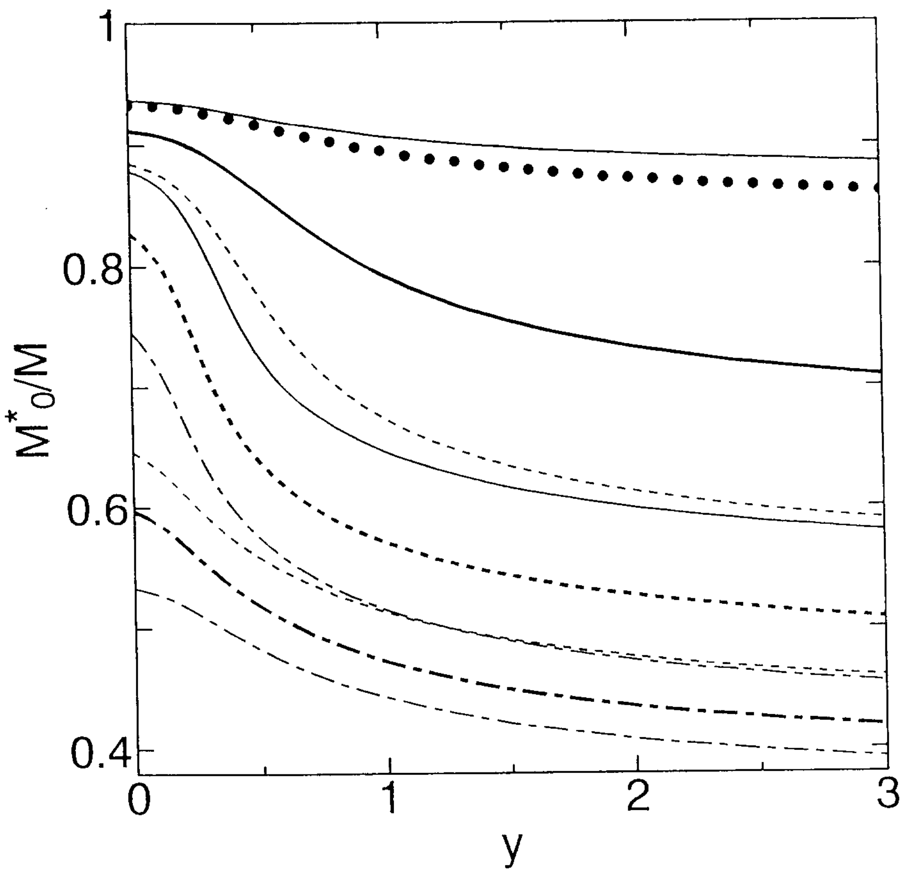

fig.6

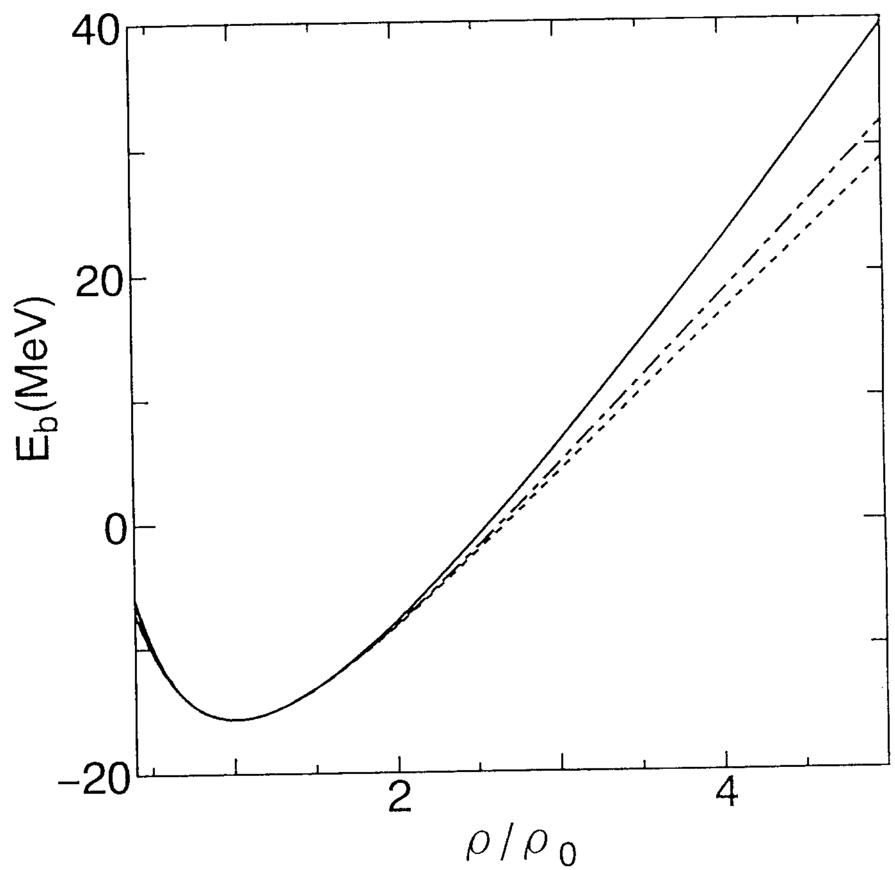

fig.7

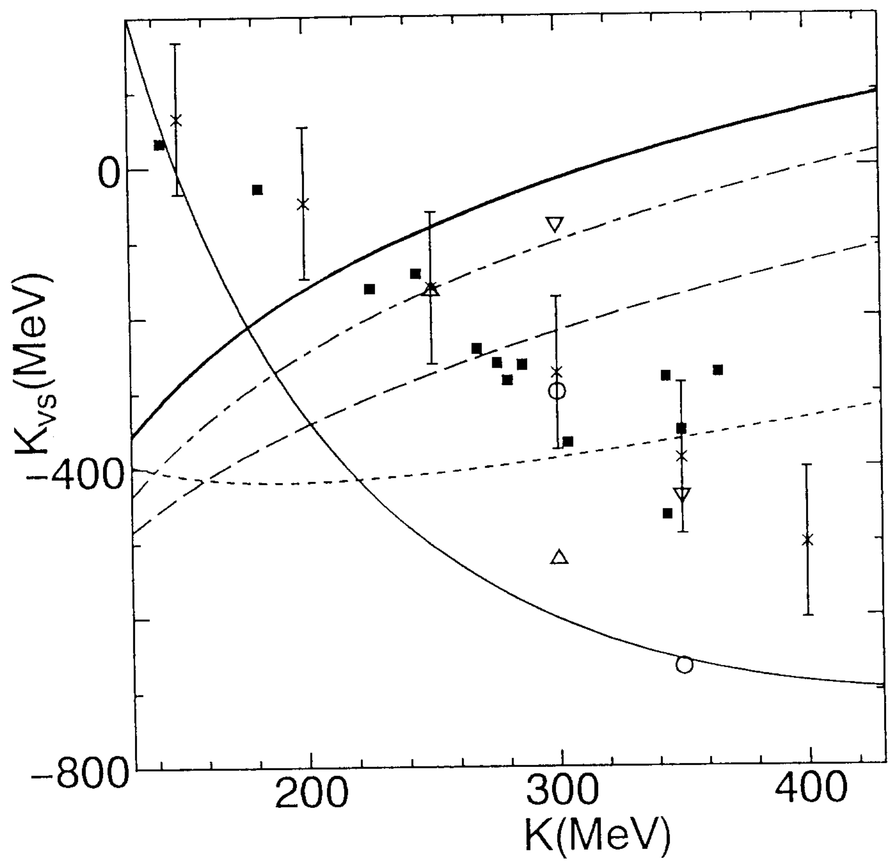

fig.8

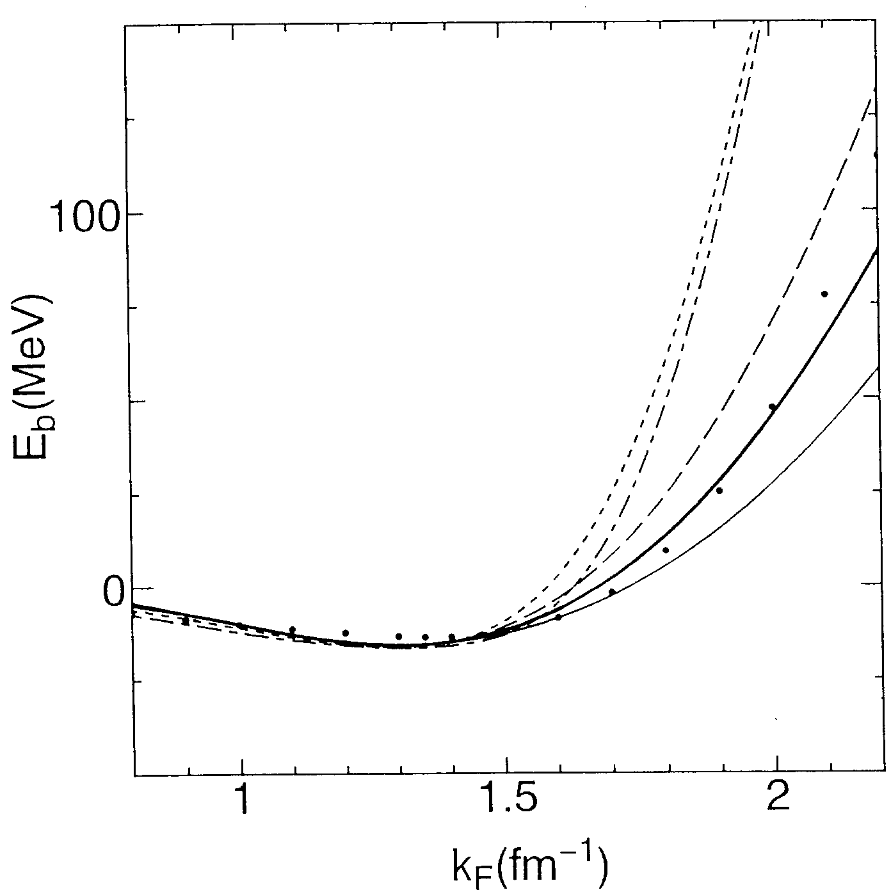

fig.9

... small solid circles are the DBHF results from the ref. [14].

Fig. 4 The $K-K'$ relation. (a)The $M_0^* = 0.6M$ case. (b)The $M_0^* = 0.8M$ case: The solid line, the dotted line, the dashed line, the dashed-dotted line, bold solid line and

Table and Figure Captions

Table I

The empirical K-K_c relation in the table of the ref. [2]. (Shown in MeV.)

Table II

Parameter sets fitted for the empirical value of K and K_c in the table I. The K, K_c, K', K_{vs}, L and K_{sym} are shown in MeV. Except in EOS 6, $C_\rho^2 = g_\rho M/m_\rho = 75.17$. In EOS 6, $C_\rho^2 = 74.69$.

Fig. 1 The y-C_v^2 relations with several values of M_0^*: The solid line, the dotted line, the dashed line, the dashed-dotted line and the bold solid line are results with M_0^*/M =0.5, 0.6, 0.7, 0.8 and 0.9 respectively.

Fig. 2 The region for $C > 0$ in the $K - M_0^*$ plane: The solid line, the dotted line, the dashed line, the dashed-dotted line, the bold solid line, the bold dotted line and the bold dashed line are results with $y = 0$, 0.1, 0.2, 0.3, 0.5, 1.0 and 2.0 respectively. In all cases, $C > 0$ above the line and $C < 0$ below the line.

Fig. 3 The $M_0^* - K'$ relation. (a)The $y = 0$ case. (b)The $y = 1.0$ case: The dashed-dotted line, the solid line, the dotted line, the dashed line and the solid triangles are the results with K =150, 200, 250, 300 and 350MeV respectively.

Fig. 4 The $K - K'$ relation. (a)The $M_0^* = 0.6M$ case. (b)The $M_0^* = 0.8M$ case: The solid line, the dotted line, the dashed line, the dashed-dotted line, bold solid line and bold dotted line are the results with y =0, 0.1, 0.5, 1.0, 2.0 and 3.0 respectively.

Fig. 5 The $K - K_c$ relation. (a)The $y = 0$ case. (b)The $y = 1.0$ case: The solid triangles, the dotted line, the dashed line, the dashed-dotted line and the solid line are the results with M_0^*/M =0.5, 0.6, 0.7, 0.8 and 0.9 respectively. The crosses with error bars are the data from the table 3 in ref. [2]. The solid small squares are the data from the table IV in ref. [3]. (For simplicity of the figure, we omit the error bars in the latter data.)

Fig. 6 The $y - M_0^*$ relation for the empirical $K - K_c$ relation: The solid small circles are the results for $K = 200$MeV and $K_c = 2.577 - 2.06$MeV. The solid lines, the dotted lines and the dashed-dotted lines are the results for K =250, 300, 350 respectively. In each case, the upper line is the result with the upper bound for K_c, the lower line is the result with the lower bound for K_c and the bold line is the result with the average value of K_c.

Fig. 7 The $\rho - E_b$ relations: The solid line, dotted line and dashed-dotted line are the results with the parameters with y =0, 0.5 and 1.0 respectively, when $K = 250$MeV and $K_c = -0.7065$MeV are satisfied.

Fig. 8 The $K - K_{vs}$ relation: The open triangles with $K = 250$ and 300MeV are the results of EOS 1 and 4 respectively. The open inverse-triangles with $K = 300$ and 350MeV are the results of EOS 2 and 5 respectively. The open circles with $K = 300$ and 350MeV are the results of EOS 3 and 6 respectively. The solid line, the dotted line, the dashed line, the dashed-dotted line and the bold solid line are the results with y =0, 0.5, 1.0, 2.0 and 5.0 respectively, when $M_0^* = 0.6M$. The crosses with error bars are the data from the table 3 in ref. [2]. The solid small squares are the data from the table IV in ref. [3]. (For simplicity of the figure, we omit the error bars in the latter data.)

Fig. 9 The $k_F - E_b$ relations for several EOS: The solid line, the bold solid line, the dashed line, the dashed-dotted line and dotted line are the results of EOS 1, EOS 3, EOS 5, the EOS with the NL parameters [20] and the EOS with NL-SH parameters [21], respectively. The small solid circles are the DBHF results from the ref. [14].